Engineering of crystal surfaces and subsurfaces by framework biomineralization protein phases. Electronic supplementary information.

Eric P. Chang,[a] Jennie A. Russ,[b] Andreas Verch,[c] Roland Kroger,[c] Lara A. Estroff,[b] and John Spencer Evans[a*]

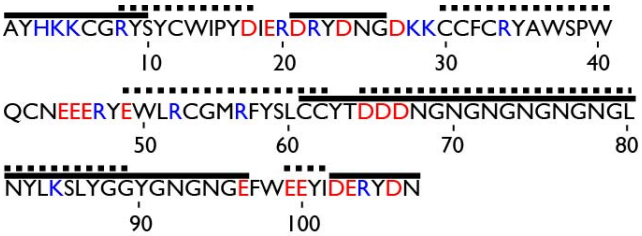

Fig S1: Primary sequence and bioinformatics analysis of the mature, processed n16.3 protein (UniProt accession number Q9TW98). Predicted regions of intrinsic disorder sequence regions (solid lines) and cross-beta strand sequence regions (dashed lines) were taken from reference 1. Negative (red) and positive (blue) charged amino acids are indicated.

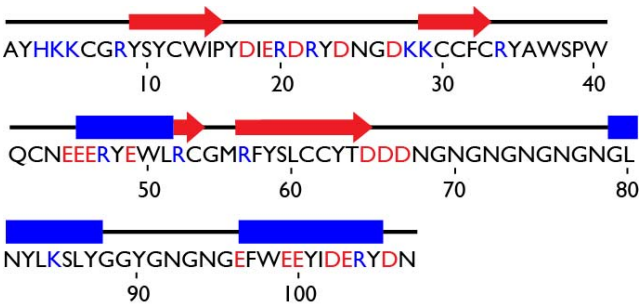

Fig S2: Primary sequence of the n16.3 protein showing predicted locations of alpha helix (red arrows), beta strand (blue rectangles), and random coil structure (black lines). Negative (red) and positive (blue) charged amino acids are indicated. Adapted from reference 2.

Experimental Section

Mineralization assays. Recombinant n16.3 (r-n16.3, MW = 7565 Da) was prepared and purified as described elsewhere.[1,2] Stock concentrations of r-n16.3 were prepared using unbuffered deionized distilled water. Mineralization assays were adapted from published protocols.[2-4] and were conducted by mixing equal volumes of 20 mM $CaCl_2$*$2H_2O$ (pH 5.5) and 20 mM $NaHCO_3$ / Na_2CO_3 buffer (pH 9.75) to a final volume of 500 µL in sealed polypropylene tubes and incubating at room temperature for 1 min, 5 min, 15 min, and 1 hr. An aliquot of r-n16.3 stock solution was added to the calcium solution prior to the beginning of the reaction, with final protein assay concentration = 10 or 30 µM, similar to that utilized in previous studies.[1,2] The final pH of the reaction mixture was measured and found to be approximately 8.0 - 8.2. Mineral and protein deposits formed during the assay were captured on 5 x 5 mm Si wafer chips (Ted Pella, Inc.) that were placed at the bottoms of the vials. Upon completion of a mineralization assay, the Si wafer was rinsed thoroughly with calcium carbonate saturated methanol and dried overnight prior to analysis.

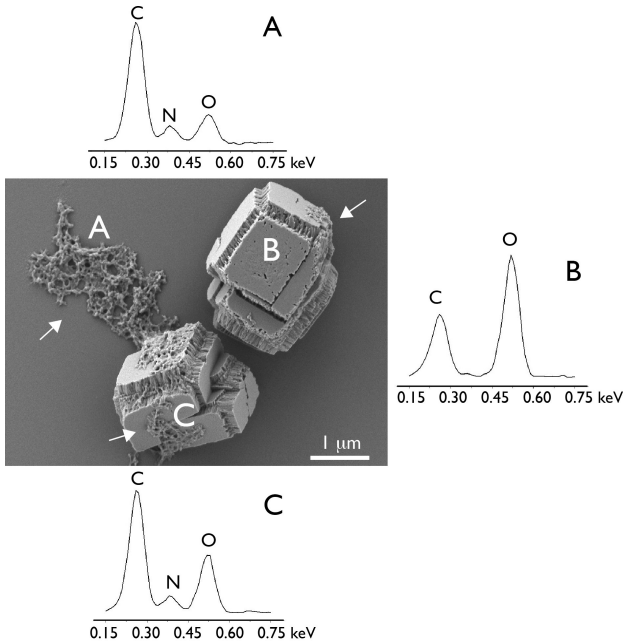

Fig S3. Representative SEM image and corresponding x-ray microanalyses of mineral and protein deposits rescued from r-n16.3 assays (15 min, 10 µM r-n16.3). Letters denote regions of EDS sampling. (A) putative protein deposit on Si wafer. (B) An exposed area of the {104} surface where no visible evidence of protein deposit could be found. (C) Protein deposit in contact with the {104} surface. Note detection of N and C:O ratios where protein gel-like deposits are observed.

Scanning Electron Microscopy. Imaging of the Si wafers extracted from the mineralization assays was performed using a Merlin (Carl Zeiss) field emission SEM (FESEM) using either an Everhart-Thornley type secondary electron detector (SE2) or an annular secondary electron detector (in lens) at an accelerating voltage of 1.5kV and a probe current of 300 pA. Prior to analysis, samples were coated with iridium using a Cressington 208HR sputter coater with thickness controller attachment. X-ray microanalysis of the iridium coated Si wafers was performed using an Oxford Instruments EDS with integrated INCA software attached to the Merlin FESEM (**Fig S3**). To perform the analysis, samples were lowered to a working distance of 8.0 mm and the acceleration voltage and probe current were increased to 2.0 kV and 1.2 nA, respectively. Areas of interest were scanned for 100 seconds each.

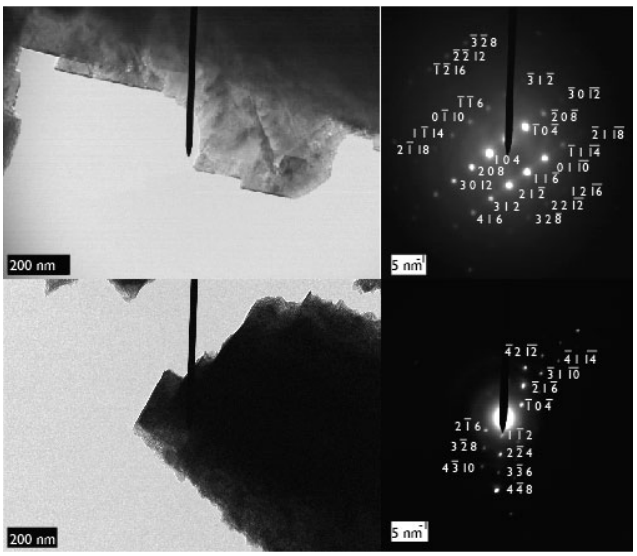

Fig S4: Representative TEM images of 30 μM r-n16.3-generated crystal assemblies rescued from 1 hr assays and corresponding single crystal electron diffraction patterns with hkl assignments.

Transmission electron microscopy and selected area electron diffraction. Crystals from the mineralization assays were extracted from the mineralization reaction vials using 0.2 micron filtered calcium carbonate saturated methanol and pipetted onto 200 square mesh gold grids coated with a formvar carbon film (Electron Microscopy Sciences, USA). TEM and electron diffraction were performed using a Philips CM12 transmission electron microscope equipped with a tungsten filament electron beam source. All imaging and diffraction analyses were performed at 120 keV. A diffraction pattern of a polycrystalline gold standard was used as a calibration scale for all subsequently recorded diffraction patterns. The selected area diffraction patterns were analyzed and indexed using ImageJ and the JEMS software package (**Fig S4**).

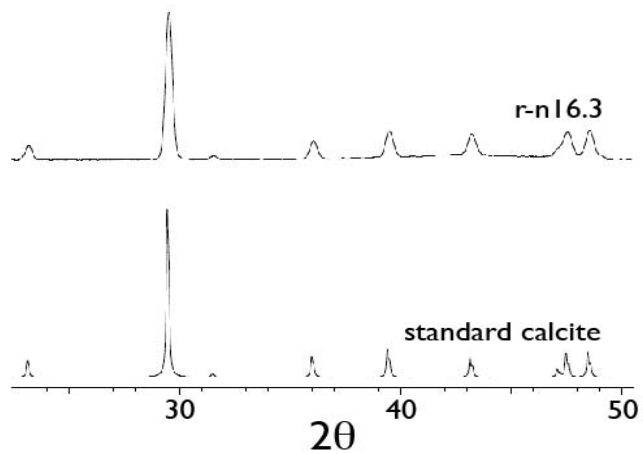

Fig S5: Micro x-ray diffraction powder pattern of bulk mineral deposits sampled from 1 hr r-n16.3 mineralization assays. The standard x-ray diffraction spectra for calcite is presented for comparison.

X-ray Diffraction (XRD). Micro x-ray diffraction analysis was performed on the bulk mineral samples captured on Si wafers obtained from the mineralization reactions prior to being coated with iridium and analyzed with FESEM. XRD measurements were performed on a Bruker AXS D8 GADDs Powder X-ray Diffractometer equipped with a Vantec-2000 area detector. Samples were scanned over a broad range of 2Θ values for 45 minutes each by oscillating and rotating the sample over a central area of approximately 1.8 mm x 1.8 mm on the Si wafer. The raw XRD data was processed, smoothed, and baseline subtracted using the Bruker AXS Eva DiffracPlus software program. These data were then compared to standard calcite, aragonite, and vaterite xrd powder pattern spectra for assignments (**Fig S5**).

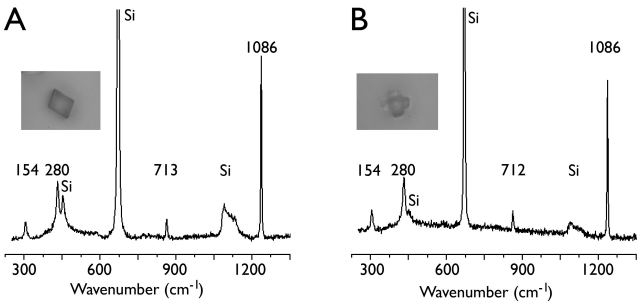

Fig S6: Representative Raman microscopy of mineralization assay material collected on Si wafers from (A) control and (B) 30 μM r-n16.3 mineralization assays, with corresponding light microscopic images of the deposits that were examined. Note that the Si wafer peaks do not overlap with any of the calcium carbonate – specific peaks. The Raman modes for synthetic aragonite, calcite and vaterite can be found in Table S1.[5]

MicroRaman analysis of mineral deposits. Si wafers containing washed and dried precipitated assay deposits were analyzed using a Renishaw InVia Raman microscope at Cornell University. Spectra were acquired under a 100X microscope objective with a laser excitation wavelength of 785 nm at 50% power (~4 mW), a 1200 line/mm grating, and a spot size of less than 1 micron (**Fig S6**).

Table S1: Raman band assignments for $CaCO_3$ polymorphs

Mode	Calcite (cm^{-1})	Vaterite (cm^{-1})	Aragonite (cm^{-1})
Lattice	156, 283	118, 268, 301	154, 208, 273
ν_1	1086	1074, 1089	1086
ν_2	---	874	854
ν_3	1435	1445, 1485	1462, 1574
ν_4	713	738, 750	704, 717
Overtones	1749	1749	---

Adapted from reference 5. Legend to table: ν_1 = symmetric stretch; ν_2 = out-of-plane bending; ν_3 = asymmetric stretch; ν_4 = in-plane bending

Focused Ion Beam Milling (FIB). The analysis of internal crystal morphology (**Fig S7**) was performed using a Zeiss Auriga Small Dual-Beam FIB-SEM. Samples prepared

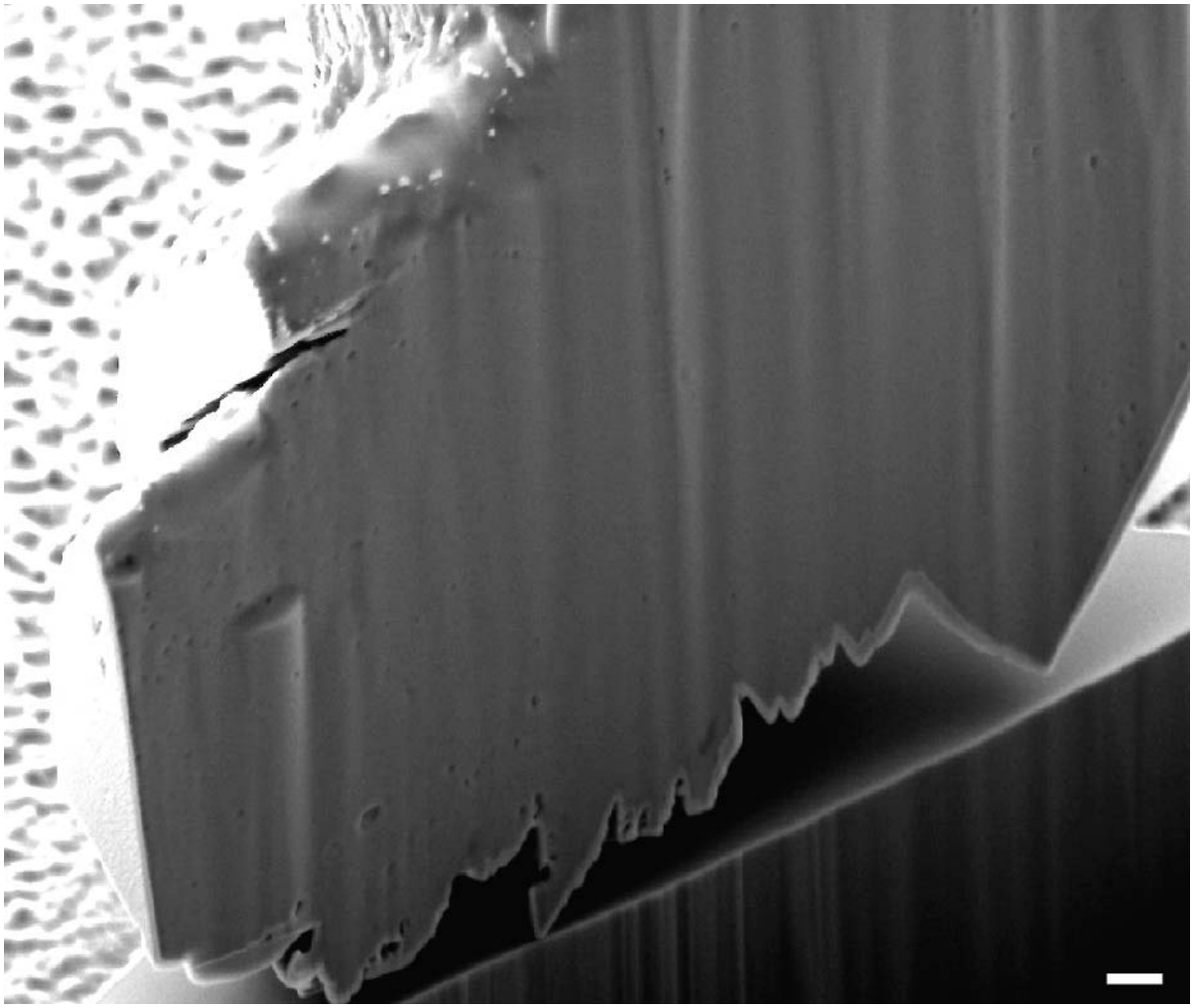

Fig S7. Enlargement of r-n16.3 -generated crystal FIB cross-section showing nanoporosities (image is the same as that shown in Fig 2). Scalebar = 200 nm.

for SEM imaging on the Zeiss Merlin were compatible with the Zeiss Auriga. All samples were coated with additional iridium prior to performing FIB. A 30 kV gallium ion beam was utilized to mill for depths of 10 – 15 mm below the beam focal point at 1 nA for coarse milling and 120 pA for fine milling. The gallium ion beam was oriented perpendicular to the sample by tilting the sample stage to 54˚. SEM images of cross-sectioned surfaces were obtained using a 2.0 kV, 600 pA electron beam and a secondary electron detector at a working distance of 5.0 mm. Images were taken shortly after cross sectioning to limit the exposure of the uncoated surfaces to the electron beam. Images of surfaces containing electron beam damage were created for comparison to images of undamaged surfaces but were not used for the purposes of discussion in this publication.

1 I. Perovic, E.P. Chang, M. Lui, A. Rao, H. Coelfen, J.S. Evans, *Biochemistry* 2014, **53**, 2739

2 C.B. Ponce, J.S. Evans, *Crystal Growth and Design* 2011, **11**, 4690.

3 C.J. Stephens, Y.Y. Kim, S.D. Evans, F.C. Meldrum, H.K. Christenson, *J. Am. Chem. Soc*. 2011, **133**, 5210; C.J. Stephens, S.F. Ladden, F.C. Meldrum, H.K. Christenson, *Adv. Mater*. 2010, **20**, 2108.

4 D. Gebauer, A. Volkel, H. Cölfen, *Science* 2008, **322**,1819.

5 M. Ndao, E. Keene, F.A. Amos, G. Rewari, C.B. Ponce, L. Estroff, J.S. Evans, *Biomacromolecules* 2010, **11**, 2539.